Kovove Mater. 62 2024 1–12
DOI: 10.31577/km.2024.1.1

Microstructure and mechanical properties of fibre laser welded joints of CP780 and TRIP690 steel

Pavol Švec[1]*, Alexander Schrek[1], Mária Dománková[2]

[1]*Institute of Technologies and Materials, Faculty of Mechanical Engineering, Slovak University of Technology in Bratislava, Námestie slobody 17, 812 31 Bratislava, Slovak Republic*
[2]*Institute of Materials Science, Faculty of Materials Science and Technology in Trnava, Slovak University of Technology in Bratislava, Bottova 25, 917 24 Trnava, Slovak Republic*

Received 14 July 2023, received in revised form 29 September 2023, accepted 3 October 2023

Abstract

Fibre laser welding of CP780 and TRIP690 steel sheets with a thickness of 1.5 mm was evaluated. Sound welds were obtained at the heat input from 43.3 to 95.0 J mm^{-1}. The highest 488 and 476 HV0.1 microhardness values were measured in the coarse-grained HAZ of CP780 and TRIP690 steel, respectively. The microstructure in the fusion zone consisted mainly of martensite and lower bainite. The microstructure in the coarse-grained HAZs contained martensite, lower bainite, upper bainite, and retained austenite. The microstructure of the inter-critical HAZs consisted of martensite and ferrite with an increased portion of ferrite with the distance from the fusion zone. The softening regions were indicated in the sub-critical HAZs of both steels. Joint tensile strength exceeded the tensile strength of TRIP690 steel. The apparent elongation was concentrated mainly in TRIP690 steel because of the transformation strengthening of the weld region during the welding process.

K e y w o r d s: CP780 steel, TRIP690 steel, fibre laser welding, microhardness, microstructure

1. Introduction

Advanced high-strength steels (AHSSs) with excellent mechanical properties and zinc coatings have received significant commercial and research interest. The AHSS steels meet the great demands on high mechanical strength, sufficient stiffness, and good ductility to satisfy the requirements for external design of car bodies. This is mainly achieved with multiphase steels, such as dual phase (DP), complex phase (CP), and transformation plasticity (TRIP) steels. These steel grades can utilise several sophisticated strengthening mechanisms, including martensite transformation during straining. These steel grades, representing the first generation of AHSS, have found the most application in the body in white applications [1–6]. The DP steels exhibit dual ferrite martensite microstructure. They have been more studied and more frequently applied for car body components, compared to CP and TRIP steels, which have more complex microstructures and are more expensive [7–9]. The CP steels derive their balanced properties from complex ferrite, bainite, and martensite microstructure. They possess high yield strength, good resistance to edge cracking, bending properties, and toughness. The CP steels are used in various automobile structures, such as stiffeners, door impact bars, seat mounting rails, and chassis components [10–12]. The TRIP steels have an excellent combination of strength and ductility. They can be considered a composite material composed of a soft matrix represented by ferrite and retained austenite and a hard phase represented by martensite and bainite. Transformation of retained austenite to martensite during deformation causes the TRIP effect, resulting in the redistribution of stress and combined effects of work hardening rate, ductility, and formability. The tensile strength and elongation of TRIP steels are usually in the range of 500 to 1000 MPa and from 30 to 15 %, respectively [1, 2, 13, 14]. Due to the high uniform elongation, there is

*Corresponding author: tel.: +421 905326211; e-mail address: pavol.svec@stuba.sk

usually a possible residual deformation capacity after drawing. This makes TRIP steel greatly beneficial for energy absorption and better in car crash situations than other AHSS grades. Because of their high strength and ductility and good impact absorption formation, TRIP steels are widely used in anti-collision components, such as frame rails, reinforcing plates, absorption boxes, roof rails, engine cradles, front and rear rails, seat frames, and anti-collision beams [2, 5, 13, 15–20].

An important utilisation of AHSSs in car body design is associated with their applications for tailor-welded blanks (TWBs). The TWBs are blanks of differing materials and/or treatments, thicknesses, or surfaces, which are generally welded before the stamping operations to improve product performance. They offer a part that increases fuel efficiency while allowing for ease of manufacturability, performance, and styling. Using TWBs to adapt locally to different loading conditions or other requirements in the part is possible. The most important advantage of parts-made TWBs is the weight reduction compared to conventional products, which could achieve 25 % when AHSSs are incorporated in TWB design [1, 21]. Other advantages of joining before the forming are the reduction of the required forming tools, the higher accuracy in the forming process, and the enhanced use of material, which leads to lower production costs. Since TRIP steels have high strength combined with improved ductility, these steel grades may be utilised in TWB car body parts with demands on energy absorption and high strength characteristics. However, CP steels may be used in car body parts with a desire for even higher strength but reduced ductility [1, 21–24].

Fibre laser welding is efficiently used to join different automobile panels in TWBs because of its favourable properties. The fibre laser welding process offers significant advantages, such as high efficiency, high energy density, low heat input, strong adaptability, and reliability in manufacturing compared to other welding processes, such as resistance spot welding, gas metal arc welding, and electron beam welding [4, 21, 23, 25]. Deep penetration can be easily achieved without the filler metal using fibre lasers. A fibre laser beam is characterised by a concentrated heat source, which significantly reduces the width of the fusion zone (FZ) and heat-affected zones (HAZs); thus, the strength of the joint usually achieves a level identical to the base metal (BM). Moreover, the welding blank deforms only slightly due to low residual stress. These characteristics of fibre laser welding enable fabricating dissimilar steel welded joints with high strength and good ductility [4, 21]. Several studies have been carried out to understand the effects of laser welding parameters on the properties of AHSSs. The welding parameters play a significant role in determining the quality of a weld joint, which can be generally defined in terms of properties such as weld bead geometry, distortion, strength, ductility, and formability. These properties and the microstructure of joints depend on the chemical composition of BMs, weld line orientation, thickness ratio of the blanks, and welding parameters, such as beam power, welding speed, and heat input [5, 21–23, 25].

Recently, many studies have been devoted to laser welding of different grades of DP steels [7–9, 25], and several studies have been devoted to laser welding of DP steels with TRIP steels [13, 16] or CP steels [11]. However, information about laser welding of TRIP steels with CP steels is still rare. Therefore, more research is needed on this interesting topic. Although information on a chosen couple of welded materials (CP with TRIP steels) is missing, some useful knowledge can be found about the HAZs of these steels when researching laser welding of identical steel grades (CP, TRIP) or these steel grades with other types, mainly DP steels.

Useful information about the laser welding of CP steels can be found in [10–12]. Morawiec [12] welded CPW 800 steel sheets with a thickness of 2.5 mm with a Yb:YAG solid-state laser. The microstructure of steel CPW 800 BM consisted of the ferritic-bainitic matrix with martensitic-austenitic islands of various sizes. The microstructures of the FZ contained lath martensite with the greatest hardness of 393 HV1. The microstructure of the HAZ was composed of fine lath martensite. The transition zone between the HAZ and the BM was characterised by a mixture of fine-grained ferrite, bainite, martensite, and retained austenite. The content of ferrite grew along with a decreasing distance from the BM. The presence of retained austenite in the form of characteristic polygonal grains was greater than that observed in the base material, which can be attributed to enrichment with carbon in the range of inter-critical temperature [12]. Pramanick [10] laser welded CP1200 steel sheets. The fine-grained HAZ showed fine bainite and martensite with some untransformed ferrite, while the inter-critical HAZ was mainly comprised of bainite and ferrite with some martensite [10]. In the work [11], CP780 and DP980 steel were fibre laser welded. The microstructures of coarse-grained HAZ of CP780 steel contained a major portion of martensite and a minor portion of lower bainite with a maximal hardness of 463 $HV_{0.1}$. In the fine-grained region of HAZ of CP780 steel, the microstructure consisting of martensite, ferrite, and lower bainite was observed at higher peak temperature and the microstructure consisting of ferrite, tempered martensite, and MX carbonitrides was observed at lower peak temperature. The softening region in HAZ of CP780 was characterised by a minimum hardness value of 237 $HV_{0.1}$ [11].

Several authors studied the laser welding of TRIP steels. Most of the papers were devoted to the

Table 1. Maximal concentration (wt.%) of alloying elements in CP780 and TRIP690 steel

Steel	C	Mn	Si	Al	P	S	V	B	Cr + Mo	Nb + Ti
CP780	0.18	2.2	0.8	2.0	0.08	0.015	0.2	0.005	1.0	0.15
TRIP690	0.32	2.5	2.2	2.0	0.12	0.015	0.2	0.005	0.60	0.20

laser welding characteristics of TRIP780 [17, 23] and TRIP800 steels [13, 15, 19], but some authors also studied the TRIP steels with a tensile strength of 600 MPa [18] and above 1000 MPa [2, 26]. As they welded either the same grade of TRIP steels or TRIP steels with DP steels, the results regarding the HAZs of TRIP steels are mainly comparable to our research. Wu [17] laser welded the TRIP780 steel sheet with a hardness of 283 HV and a thickness of 1.4 mm to the QP1180 steel sheet with a thickness of 1.2 mm. Both coarse-grained and fine-grained HAZ on the TRIP780 side were fully martensite and had a hardened zone. The inter-critical HAZ of the TRIP780 consisted of ferrite, martensite, and a small amount of retained austenite. The microstructure of the sub-critical HAZ of the TRIP780 was composed of ferrite, bainite, tempered martensite, a small amount of cementite, and retained austenite. In the sub-critical HAZ, the austenite volume fraction decreased, but the martensite volume fraction increased compared with the TRIP780 BM, which resulted in no obvious HAZ softening. This was related to the balance of martensite tempered ratio and decomposition ratio RA to martensite [17]. Other authors reported HAZ softening in the sub-critical region and attributed it to martensite tempering [2, 13]. Mujica [19] welded TRIP800 with a thickness of 1 mm and hardness of 250 $HV_{0.05}$ with TWIP steel 1.5 mm thick sheet using Nd:YAG laser. HAZ of the TRIP steel had a hardness ranging from 350 to 450 $HV_{0.05}$, attributed to the high-volume fraction of martensite and the small grain size [19]. Rossini [13] used an Nd-YAG laser for welding TRIP steel with a thickness of 0.8 mm and hardness of 240 HV30 to TWIP and DP steel. The retained austenite on the TRIP side was transformed into martensite in the HAZ, but no bainite was detected. The softening of the DP and TRIP steels in the HAZ close to the BM was observed and was attributed to the sub-critical tempering of the original microstructure [13]. Guzman-Aguilera [15] butt-welded monolithic Si-TRIP steel sheets with a strength of 800 MPa and a thickness of 1.0 mm by employing fibre laser welding. He observed the formation of predominantly martensite with a hardness of 520 ± 17 HV in both FZ and HAZ [15]. Lang [18] laser welded TRIP steel with a strength of 600 MPa using Nd:YAG pulsed solid-state laser. Acicular cementite, massive ferrite, layered pearlite, and granular bainite were mainly observed in the joint [19]. In the work [27], TRIP690 and 340LAD steel were fibre laser welded. The microstructure in the coarse-grained HAZ of TRIP690 steel was built mainly of martensite and lower bainite with a maximal hardness of 457 $HV_{0.1}$. In the fine-grained HAZ of TRIP690 steel, the microstructure consisted of martensite, lower bainite, and ferrite. The ferrite portion increased with the distance from the weld centre and with a decrease in the maximal temperature achieved during the welding cycle in the inter-critical temperature interval. The smallest value of 214 $HV_{0.1}$ in the HAZ of TRIP690 steel was in the vicinity of TRIP690 steel BM and represented the softening region of sub-critical HAZ [27].

From the information above, it is obvious that significant differences can be found when describing the microstructure in HAZs of CP and TRIP steel grades. Some authors claim fully martensitic microstructure in the coarse-grained upper-critical HAZs [12, 17, 19], but others observed more complex microconstituents [10, 11, 19, 27]. Some authors observed the softening regions in the sub-critical HAZs [2, 11, 13, 27]; others didn't identify them [17]. So, the present research focused on the microstructure and mechanical properties of fibre laser welded joints of CP780 and TRIP690 steel could contribute to this research.

2. Experiment

The complex phase steel CP780 and transformation-induced plasticity steel TRIP690, which had the same thickness of 1.5 mm, were chosen for the fibre laser welding experiments. The sheets of these steels had the same zinc coating of 100 g m^{-2}, but they differed in chemical composition, as listed in Table 1. The CP780 steel possesses a higher maximal concentration of Cr and Mo but a lower concentration of C and Mn in comparison with the TRIP690 steel. The basic mechanical properties of BMs are compared in Table 2. As the CP780 steel is special for its strength and the TRIP690 steel is characterised by its elongation, they were chosen to utilise their different stress-strain potential when joining TWB parts for car body production.

Butt welds were fibre laser welded using sheets of experimental AHSSs with a length of 200 mm and a width of 100 mm. The longitudinal edges of the sheets were milled before welding to minimise the gap between the welded edges. The ytterbium solid-state fibre laser IPG YLS-5000 with a maximum output of 5000 W, wavelength of 1060 nm, and fibre diam-

Table 2. Mechanical properties of CP780 and TRIP690 steel

Steel	Proof strength (MPa)	Tensile strength (MPa)	Elongation (%)
CP780	500–700	min. 780	min. 10
TRIP690	430–550	min. 690	min. 23

Table 3. Parameters of fibre laser welding

Weld No.	1	2	3	4	5	6	7	8	9	10	11
v (mm s^{-1})	10	20	30	40	50	60	70	80	100	100	120
P (W)	950	1200	2200	2300	2700	3200	3400	4500	5000	4700	5200
f (mm)	+7	+10	+12	+10	+10	+10	+7	+10	+7	+10	+6
P/v (J mm^{-1})	95.0	60.0	73.3	57.5	54.0	53.3	48.6	56.3	50.0	47.0	43.3

eter of 100 µm was applied for welding without filler metal and a shielding atmosphere. The welding head PRECITEC YW52 was used to lead the laser beam source along a linear welding trajectory at a distance of 250 mm from the welded lines. The process parameters applied during the fibre laser welding are summarised in Table 3. Gradational welding speeds (v) were chosen in the interval from 10 to 120 mm s^{-1} to study the effect of welding parameters on the joint properties. The beam power (P) in the interval from 950 to 5200 W and focus (f) from + 6 to + 12 mm was optimised for every welding speed to achieve proper weld line form. Maximal theoretical heat input calculated as P/v changed from 95.0 to 43.3 J mm^{-1} when increasing the welding speed from 10 to 120 mm s^{-1} and the beam power from 950 to 5200 W.

The stereomicroscope Zeiss was used to adjust welding parameters to prepare the required weld line geometry and study the surfaces of the laser welds. The transverse cross-section samples were cut off the fibre laser welded joints and prepared for microstructure observation. The microstructures were observed using an Axiovert 40MAT light microscope. The grain size was measured by image analysis using the Multiphase module of AxioVision software. Scanning electron microscopy (SEM) observation using a JEOL JSM-IT300 microscope and energy dispersive spectroscopy (EDS) analysis using an Oxford Instruments X-Max 20 spectrometer were used to characterise the joint microstructures. Transmission electron microscopy (TEM) analysis of joints was performed using both the JEOL 200 CX microscope with an accelerating voltage of 200 kV and the Philips CM 300 microscope with an accelerating voltage of 300 kV. The TEM samples in the form of carbon extraction replicas and thin film samples were prepared for this analysis, and observed phases were identified by the selected area electron diffraction (SAED).

The microhardness profiles were measured across the welded joints parallel to the surfaces of sheets using a Vickers indenter with a load of 100 gf (0.98 N) at a distance of 0.1 mm between the indentations. The samples for tensile tests with the geometry documented in Fig. 12 were prepared from the fibre-welded joints. The universal testing machine Instron 195 with a crosshead speed of 50 mm min^{-1} was used for tensile tests of joints.

3. Results

3.1. Macrostructure of fibre laser welded joints

The macrostructure of fibre laser welded joints was influenced by the heat input, which is documented in Fig. 1. Two joints welded at the theoretical heat input of 53.3 J mm^{-1} (beam power of 3200 W, welding speed of 40 mm s^{-1}), and the heat input of 48.6 J mm^{-1} (beam power of 3400 W, welding speed of 70 mm s^{-1}) are compared in Fig. 1. Complete penetrations can be seen, and the sub-zones of the welds can be distinguished at these joints. The typical columnar grains are created in the FZs. The sign of rolling texture remains in both BMs. The macrographs in Fig. 1 confirm that sound laser welds were obtained without any obvious macroscopic defects, such as microvoids or cracks. However, both joints are characterised by the slight concavity of the face and root sagging. These joints are compared to present the changing microstructure shape at the heat input value of about 50 J mm^{-1}. When laser welding at the heat input above 50 J mm^{-1}, the wine glass shape is created with the face of the weld region wider than the root of the weld region. This can be seen at the joint laser welded at 53.3 J mm^{-1} in Fig. 1a. The differences in weld widths were more evident at higher heat input parameters. The maximal width of the fusion zone at the faces of joints increased from 0.9 to 2.1 mm when increasing the heat input from 43.3 to 95.0 J mm^{-1}, re-

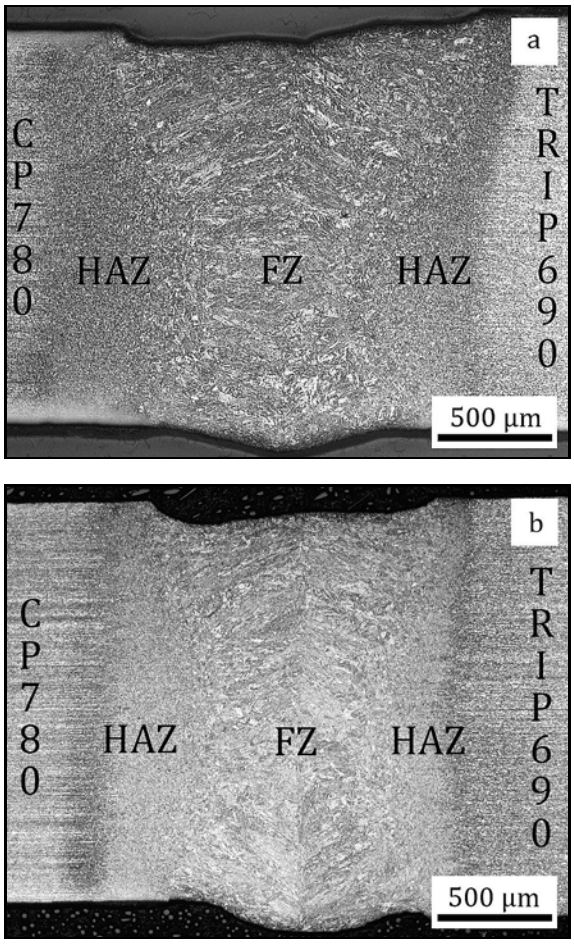

Fig. 1. Macrostructure of fibre laser welded joint of CP780 and TRIP690 steel: (a) wine glass shape at $P/v = 53.3\,\mathrm{J\,mm^{-1}}$ and (b) hourglass shape at $P/v = 48.6\,\mathrm{J\,mm^{-1}}$ (FZ – fusion zone, HAZ – heat affected zone).

spectively. The joints welded at the heat input below $50\,\mathrm{J\,mm^{-1}}$ had more uniform shapes. The joints possessed hourglass shapes with the same width of both the face and root of the joints, as can be seen for the joint laser welded at the heat input of $48.6\,\mathrm{J\,mm^{-1}}$ in Fig. 1b. The interfaces of HAZs with BMs of this joint are characterised by quite narrow shapes.

3.2. Microhardness profiles across the fibre laser welded joints

The microhardness profiles were measured across the central section of the welded joints to study the effect of welding parameters on the microhardness evolution in the FZ, both HAZs and BMs. No differences in the hardness intervals in particular sub-zones were noticed when comparing the joints prepared at different heat inputs from 43.3 to $95.0\,\mathrm{J\,mm^{-1}}$. This is presented for two joints with maximal and minimal heat input in Fig. 2. Both microhardness profiles in

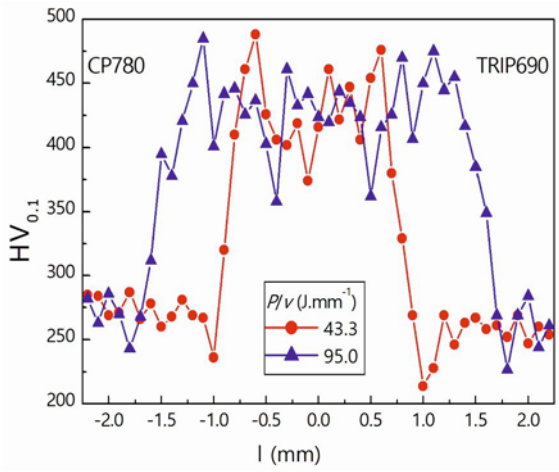

Fig. 2. Microhardness profiles across the fibre laser welded joints at minimal and maximal theoretical heat input P/v.

Fig. 2 show similar hardness intervals in identical sub-zones of these joints but with different thicknesses of these sub-zones. The microhardness profiles are characterised by increased microhardness values in both HAZs from BMs towards the FZs. The hardness of CP780 steel BM is in the interval from 260 to 299 $\mathrm{HV_{0.1}}$. However, the microhardness in the interval from 233 to 269 $\mathrm{HV_{0.1}}$ was measured for TRIP690 steel BM, which confirms the lower strength of TRIP690 steel BM compared to CP780 steel. The microhardness values in FZs of all joints were in the interval from 338 to 461 $\mathrm{HV_{0.1}}$ without any relation to the welding parameters. The microhardness in the HAZs of CP780 steel was in the interval from 234 to 488 $\mathrm{HV_{0.1}}$, and the microhardness in the HAZs of TRIP690 steel was from 205 to 476 $\mathrm{HV_{0.1}}$. The highest values in both HAZs (488 and 476 $\mathrm{HV_{0.1}}$) slightly exceeded the maximal hardness measured in the FZs, which were measured in coarse-grained regions of HAZs. The minimal hardness in the HAZs of CP780 steel was from 234 to 246 $\mathrm{HV_{0.1}}$, and it was measured in the vicinities of CP780 steel BMs and represents the softening regions of these HAZs. Similar softening regions in the HAZs of TRIP690 steel were indicated by the smallest hardness in these HAZs, from 205 to 223 $\mathrm{HV_{0.1}}$. According to the small effect of welding parameters on the microhardness values in characteristic sub-zones of joints, the fibre laser joint prepared at the theoretical heat input of $48.6\,\mathrm{J\,mm^{-1}}$ was chosen to analyse microstructure in individual sub-zones.

3.3. Microstructure of base metals

The microstructure of CP780 steel is documented in an SEM micrograph in Fig. 3. The ferritic matrix with rows of martensite and lower bainite can be

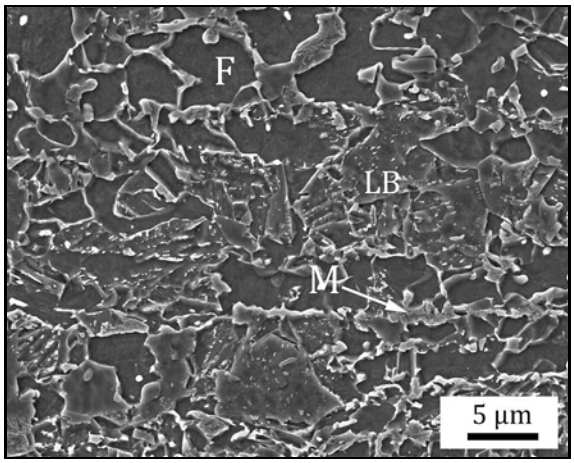

Fig. 3. Microstructure of CP780 steel BM, SEM (F – ferrite, M – martensite, LB – lower bainite).

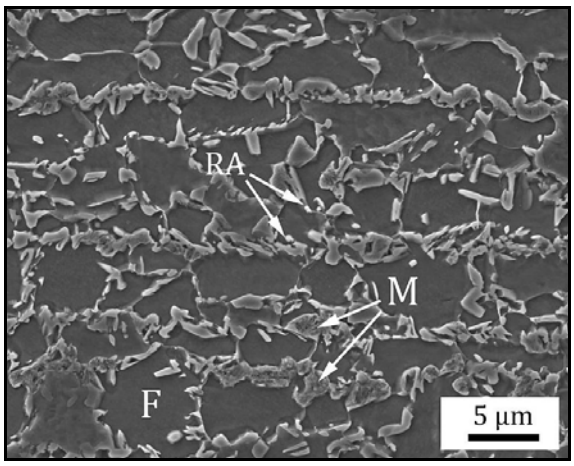

Fig. 4. Microstructure of TRIP690 steel BM, SEM (F – ferrite, M – martensite, RA – retained austenite).

seen in Fig. 3. The identification of observed microconstituents was confirmed in the work [11]. The ferrite phase was characterised by slight crystallographic texture and heterogeneity in grain size in the interval from 2 to 15 µm. However, martensite had a lath morphology and a high density of dislocations. The lower bainite had acicular morphology with a high density of dislocations. Carbide particles precipitated inside the bainitic grains. These were mainly M_3C carbides, but M_2C and MC carbides occasionally precipitated in the bainite. The hardness value in the interval from 260 to 299 $HV_{0.1}$ (see Fig. 2) corresponds well to the observed microstructure of the CP780 steel.

The SEM micrograph revealing the microstructure of TRIP690 steel BM is documented in Fig. 4. The microstructure of TRIP steel is finer compared to CP steel. It consists of a ferritic matrix of rows of martensite and a small portion of retained austenite. The ferritic grains are characterised by slight crystallographic texture sizes from 1 to 8 µm. Occasionally, the M_3C carbides precipitate mainly on the ferrite martensite interface [27]. The microhardness values in the interval from 233 to 269 $HV_{0.1}$ were measured for TRIP690 steel BM in Fig. 2. These values are slightly lower than the values of CP780 steel BM.

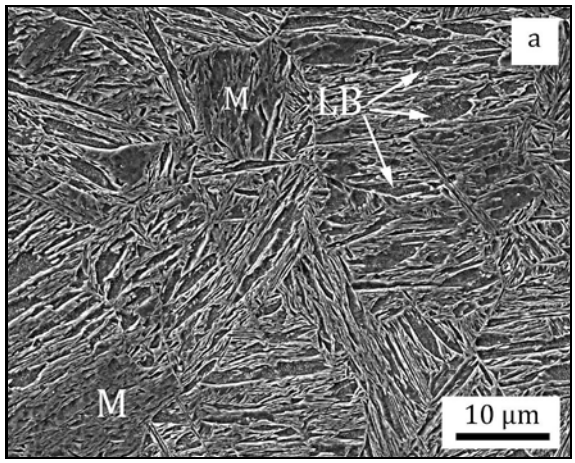

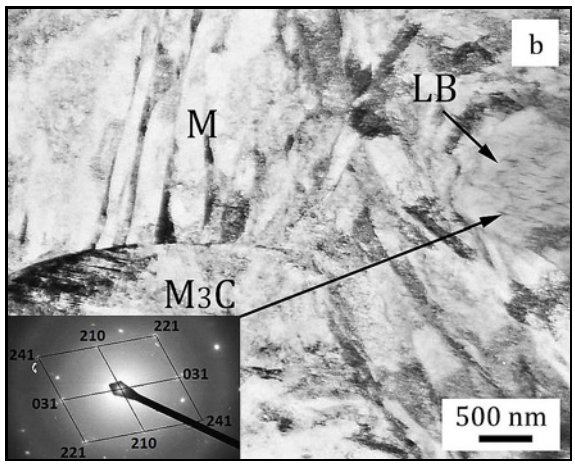

Fig. 5. Microstructure in FZ of weld: (a) SEM and (b) TEM micrograph with SAED image (M – martensite, LB – lower bainite, M_3C – carbide precipitate).

3.4. Microstructure of fusion zone of fibre laser welded joints

The microstructure in the FZ of the weld is documented by SEM micrograph in Fig. 5a and by TEM micrograph with the SAED image in Fig. 5b. The microstructure of FZ experienced the highest peak temperature above 2000 ℃ during the laser welding process. It is built by columnar grains grown opposite to the heat conduction. The microstructure consists mainly of martensite and lower bainite. This is the consequence of a high cooling rate and high content

of hardening elements, such as Mn, Cr, and Mo, in both experimental steels. A similar microstructure was observed throughout the whole FZ region. The microhardness values from 338 to 461 $HV_{0.1}$ indicate the creation of a small portion of softer microconstituents, but they were not detected. The morphological details of martensite and lower bainite phase are visible in the thin film sample in Fig. 5b. Very fine secondary particles with regular geometry were observed inside the ferritic lath. These particles were identified by SAED analysis as M_3C carbides, and their SAED image is in the bottom left part of TEM micrographs in Fig. 5b. The presence of retained austenite can be assumed at the borders of martensitic laths. Its presence could be assumed from its morphology and the character of the observed microstructure, but it could not be reliably identified by SAED analysis.

3.5. Microstructure of HAZ sub-zones of fibre laser welded joints

The microstructures of HAZ sub-zones are created by the thermal weld cycle, with different peak temperatures and cooling rates experienced during the fibre laser welding. Since the welded steel sheets have the same thickness of 1.5 mm, uniform peak temperatures can be supposed to be at identical distances from the FZ in both HAZs. Moreover, the chemical compositions of experimental steels don't differ significantly, so the microstructure differences were observed with the variation in the distances from the FZ, and fewer differences were found between identical sub-zones of HAZs. High microhardness intervals measured across both HAZs (see Fig. 2) correspond with creating different microstructures. A high portion of martensite was observed in the high-tempered regions of HAZs. With the distances from the FZ, the portions of martensite decreased, but the appearance of lower bainite, upper bainite, ferrite, and retained austenite increased.

The coarse-grained and fine-grained sub-zone can be distinguished within the upper-critical HAZ of CP780 steel. The microstructure of the coarse-grained HAZ of CP780 steel is documented in Fig. 6. Because of the long holding time at peak temperature high above A_3 critical temperature, coarsening of prior austenite grain can be observed in this sub-zone of HAZ. The grain size is in the interval from 15 to 30 μm. The microstructure consists mainly of martensite with a small portion of lower bainite, upper bainite and retained austenite. A high portion of lath martensite and lower bainite can be seen in the SEM image in Fig. 6a. Martensitic bainitic microstructure corresponds well to the maximal microhardness value of 488 HV0.1 measured in this sub-region of HAZ. However, lower microhardness values indicate the creation of softer microconstituents, such as upper bainite and

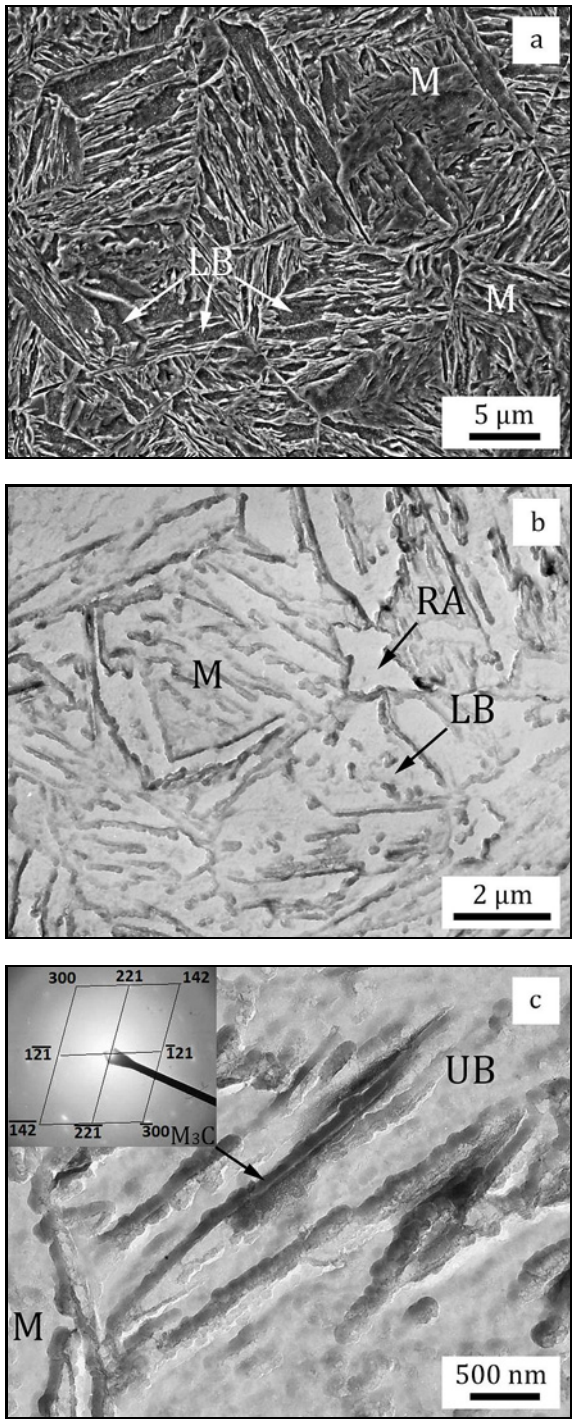

Fig. 6. The microstructures of coarse-grained HAZ of CP780C steel: (a) SEM, (b) TEM, and (c) TEM micrograph of upper bainite with SAED image (M – martensite, LB – lower bainite, RA – retained austenite, UB – upper bainite, M_3C – carbide precipitate).

retained austenite. Morphological details of martensite, lower bainite, and retained austenite can be seen in the TEM micrograph in Fig. 6b. Small M_3C carbides were identified by EDS analysis inside the laths

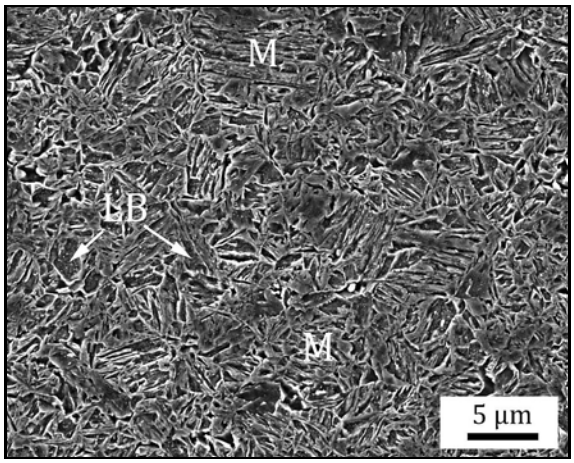

Fig. 7. The microstructure of fine-grained HAZ of CP780 steel, SEM (M – martensite, LB – lower bainite).

of lower bainite. Figure 6c documents a TEM image of upper bainite, which is occasionally created in small areas in this HAZ. Acicular M_3C carbides can be seen between the upper bainitic laths in Fig. 6c, and the SAED image of the extracted M_3C particle is a part of Fig. 6c.

The microstructure of fine-grained HAZ of CP780 is documented in Fig. 7. Lath microstructure like the microstructure in Fig. 6a is observed. The peak temperature is slightly above the A_3 critical temperature in this region. The austenitisation is still complete, but the grains are finer because of lower peak temperature and shorter time than coarse-grained HAZ. The microstructure in this fine-grained region is predominantly built of martensite and lower bainite. The identification of created microconstituents is identical to the microstructure in Fig. 6a and is confirmed by the microhardness values, which reached high values above 400 $HV_{0.1}$ in this subregion of HAZ.

The inter-critical HAZ region of CP780 steel is documented in Fig. 8. As the peak temperatures decrease with the distance from the FZ, austenitization is incomplete, and less microstructure transformation occurs. The microstructure consists of martensite and ferrite, as can be seen in the SEM micrograph in Fig. 8a and in details in the TEM micrograph in Fig. 8b. The portion of ferrite increases with the distance from FZ so with the decreasing of maximal peak temperature during the laser welding. The martensitic ferritic microstructure is also in the sub-critical HAZ. Tempering of the martensite phase can be supposed in this sub-critical HAZ, which was detected based on the microhardness decrease to the values from 236 to 243 $HV_{0.1}$. These values fall under the CP780 steel BM microhardness (from 260 to 299 $HV_{0.1}$), and these results are in good accordance with the works [11, 12].

The microstructure in the coarse-grained HAZ of

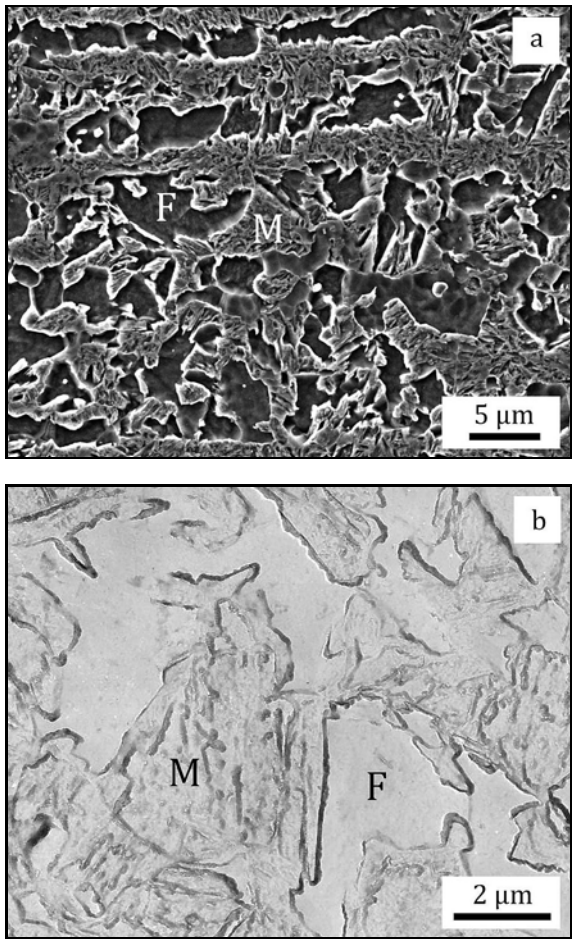

Fig. 8. The microstructures of inter-critical HAZ of CP780 steel: (a) SEM and (b) TEM (F – ferrite, M – martensite).

TRIP690 steel is documented in Fig. 9. It is characterised by coarsening prior austenitic grain with the grain size in the interval from 15 to 25 µm. This is slightly less than for CP780 steel because of the smaller original grain size of TRIP690 steel BM (Fig. 4) compared to CP780 steel (Fig. 3). The microstructure consists mainly of martensite and lower bainite with a maximal hardness of 476 $HV_{0.1}$. Martensitic laths can be seen in both SEM and TEM images in Fig. 9. Moreover, a small portion of lower bainite and retained austenite can be seen during the observation of microstructure by TEM in Fig. 9b. The morphological characteristics of observed microconstituents are identical to the microstructure of coarse-grained HAZ of CP780 steel.

The microstructure in the fine-grained HAZ of TRIP690 steel is documented in Fig. 10. In this subzone tightly heated above the A_3 transformation temperature, the fine-grained microstructure is created. The difference in grain size is evident from the comparison of the microstructure in Fig. 10 with the microstructure in the coarse-grained region in Fig. 9.

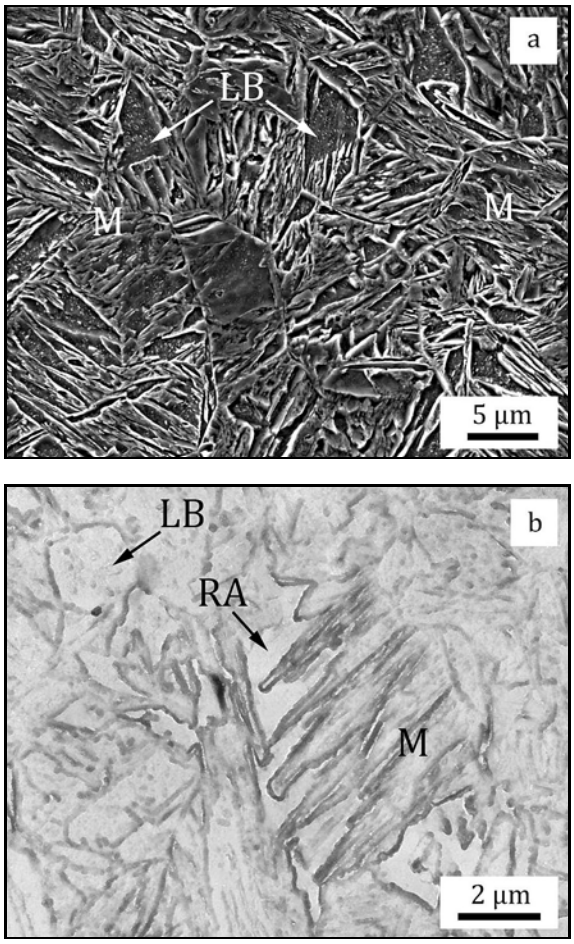

Fig. 9. The microstructure of coarse-grained HAZ of TRIP690 steel: (a) SEM and (b) TEM (M – martensite, LB – lower bainite, RA – retained austenite).

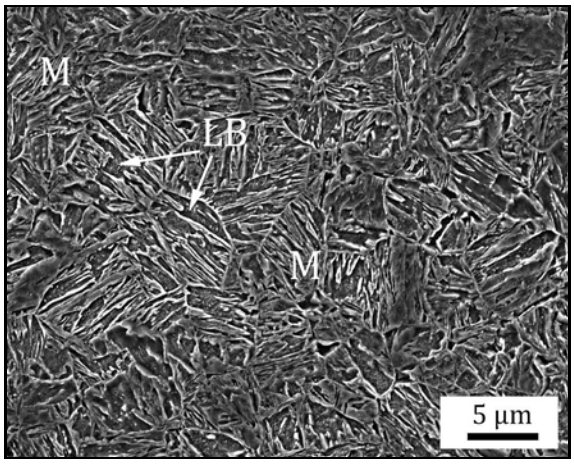

Fig. 10. The microstructures of fine-grained HAZ of TRIP690 steel, SEM (M – martensite, LB – lower bainite).

Otherwise, the created phases are similar in both subzones (Figs. 9 and 10) with identical identification criteria. The microstructure in Fig. 10 consists mainly of martensite and lower bainite and is represented by high microhardness values above 400 $HV_{0.1}$ (see Fig. 2).

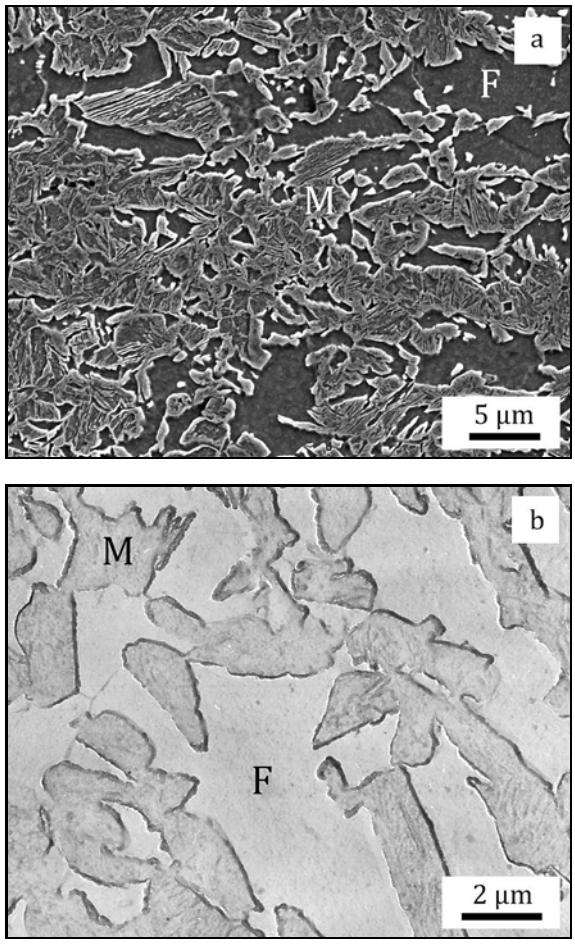

Fig. 11. The microstructures of inter-critical HAZ of TRIP690 steel: (a) SEM and (b) TEM (F – ferrite, M – martensite).

The microstructure created within the inter-critical HAZ region of TRIP690 steel is documented in Fig. 11. The microstructure consists mainly of ferrite and martensite. The portion of ferrite increases with the distance from FZ because of the decrease of maximal peak temperature and the hindering of austenitisation during the laser welding process. This is the consequence of microhardness decrease from 476 to 250 $HV_{0.1}$ with the distance from FZ. Again, the sub-critical HAZ is detected based on hardness decrease, from 233 to 269 $HV_{0.1}$ measured for TRIP690 steel BM, to the values from 205 to 223 $HV_{0.1}$. The microstructure of the sub-critical HAZ is like the structure in Fig. 11. The softening effect can be attributed to the sub-critical tempering of the original microstructure. This assumption was confirmed in works [2, 13]. The microhardness and microstructure

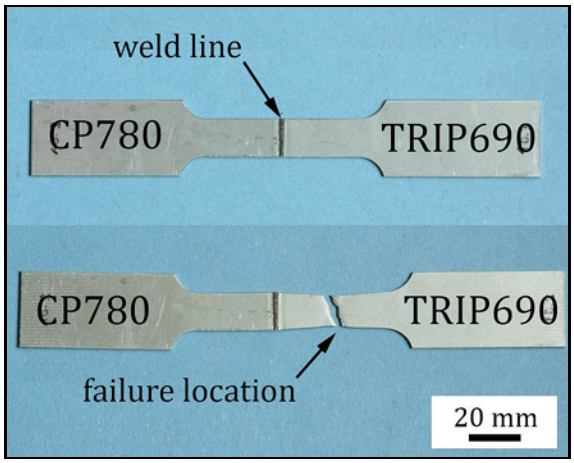

Fig. 12. Tensile sample of fibre laser welded joint of CP780 and TRIP690 steel before and after the tensile test.

results can be compared with several works [13, 17, 19, 23].

3.6. Tensile tests of fibre laser welded joints

The tensile tests confirmed the proper strength of the joints prepared at all fibre laser welding parameters. The tensile strength of all joints was in the interval from 738.7 to 756.9 MPa. This interval represents the strength of the TRIP690 steel BM because of the fracture location in this BM. The representative sample broken in TRIP690 steel BM is documented in Fig. 12. The softening zones of both HAZs did not have a negligible influence on the tensile properties. The deformation was not concentrated in these zones but mainly in TRIP690 steel BM [2]. The apparent elongation achieved the values from 16.7 to 18.2 %. It was concentrated mainly in TRIP690 steel BM because of the higher strength of CP780 steel BM compared to TRIP690 steel BM and transformation strengthening of weld region during the cooling from peak temperature after fibre laser welding. Harder microconstituents compared to the BMs were created in the welds, which was confirmed by microhardness profiles across the welded joints in Fig. 2 and microstructural analysis.

4. Conclusions

The fibre laser-welded joints of complex phase CP780 and transformation-induced plasticity TRIP690 steel were studied with respect to their macrostructure, microstructure, microhardness, and tensile properties. The sheets of experimental steels with an identical thickness of 1.5 mm were fibre welded at the theoretical heat input from 43.3 to 95.0 J mm^{-1}. Sound welds were obtained without any obvious macroscopic defects but with slight concavity of the face and root sagging at all welding parameters.

Microhardness values across the joints prepared at all fibre laser welding parameters achieved identical maximal values in particular sub-zones, but the widths of these sub-zones were different. The microhardness values in the FZs of all joints were in the interval from 338 to 461 $HV_{0.1}$. The maximal width of the fusion zone at the faces of joints increased from 0.9 to 2.1 mm when increasing the heat input from 43.3 to 95.5 J mm^{-1}, respectively. The highest microhardness interval was measured in the HAZs of CP780 steel, from 234 to 488 $HV_{0.1}$, and in the HAZs of TRIP690 steel, from 205 to 476 $HV_{0.1}$.

The microstructure of CP780 steel consisted of a ferritic matrix with rows of martensite and lower bainite. The microstructure of TRIP690 steel was finer compared to CP steel, and it was composed of a ferritic matrix and rows of martensite and retained austenite. The microstructure of FZ was built by columnar grains that grew in the opposite direction to the heat conduction. The microstructure contained mainly martensite and lower bainite.

In the coarse-grained HAZ of CP780, the coarsening of prior austenitic grain size from 15 to 30 µm was measured. The microstructure consisted mainly of martensite with a small portion of lower bainite, upper bainite, and retained austenite. The microhardness reached the highest value of 488 $HV_{0.1}$ in this subregion of HAZ. The microstructure in fine-grained HAZ of the CP780 steel region was predominantly built of martensite and lower bainite. The austenitisation was not complete in the inter-critical HAZ region of CP780 steel, and less microstructure transformation occurred. The microstructure consisted of martensite and ferrite. The ferrite portion increased with the distance from the FZ, so with the decreasing of maximal peak temperature during laser welding.

The microstructure of coarse-grained HAZ of TRIP690 steel expressed coarsening of prior austenitic grain with a grain size from 15 to 25 µm. The microstructure consisted mainly of martensite, lower bainite and a small portion of retained austenite with a maximal hardness of 476 $HV_{0.1}$. In the fine-grained HAZ of TRIP690 steel, region tightly above the A_3 temperature, the microstructure contained mainly martensite and lower bainite. However, the microstructure in the inter-critical HAZ of TRIP690 steel was composed of ferrite and martensite, and the portion of ferrite increased toward the BM.

The subcritical HAZs of both steels were detected based on the decrease in microhardness caused by subcritical tempering of the original microstructure in these HAZ regions. The lowest microhardness values in these regions were from 236 to 243 $HV_{0.1}$ for CP780 steel and 205 to 223 $HV_{0.1}$ for TRIP690 steel.

The tensile tests confirmed the proper strength of

the joints prepared at all experimental welding parameters. The tensile strength of joints achieved the value from 738.7 to 756.9 MPa, which exceeded the tensile strength of TRIP690 steel BM with all samples broken in TRIP690 steel BM. The apparent elongation in the interval from 16.7 to 18.2 % was concentrated mainly in TRIP690 steel BM because of the higher strength of CP780 steel BM compared to TRIP690 stell BM and transformation strengthening of weld region during the cooling from peak temperature after fibre laser welding.

Acknowledgements

The work was supported by the Ministry of Education, Science, Research and Sport of the Slovak Republic under the VEGA 1/0302/23 project.

References

[1] J. H. Schmitt, T. Iung, New developments of advanced high-strength steels for automotive applications, C. R. Phys. 19 (2018) 641–656. https://doi.org/10.1016/j.crhy.2018.11.004

[2] B. Zhang, Y. Dong, Y. Du, R. D. K. Mishra, H. Y. Wu, X. N. Wang, W. Z. Zhao, L. X. Du, Microstructure and formability performance of fiber laser welded 1.2 GPa grade hot-rolled TRIP steel joints, Opt. Laser Technol. 143 (2021) 107341. https://doi.org/10.1016/j.optlastec.2021.107341

[3] M. H. Razmpoosh, E. Biro, D. L. Chen, F. Goodwin, Y. Zhou, Liquid metal embrittlement in laser lap joining of TWIP and medium-manganese TRIP steel: The role of stress and grain boundaries, Mater. Charact. 145 (2018) 627–633. https://doi.org/10.1016/j.matchar.2018.09.018

[4] K. M. Hong, Y. C. Shin, Prospects of laser welding technology in the automotive industry: A review, J. Mater. Process. Technol. 245 (2017) 46–69. https://doi.org/10.1016/j.jmatprotec.2017.02.008

[5] S. S. Nayak, V. H. Baltazar Hernandez, Y. Okita, Y. Zhou, Microstructure–hardness relationship in the fusion zone of TRIP steel welds, Mater. Sci. Eng. A 551 (2012) 73–81. https://doi.org/10.1016/j.msea.2012.04.096

[6] A. Guzanová, E. Janoško, D. Draganovská, J. Viňáš, M. Tomáš, J. Brezinová, S. Maláková, M. Džupon, M. Vojtko, Metallographic study of overlapped laser welds of dissimilar materials, Metals 12 (2022) 1682. https://doi.org/10.3390/met12101682

[7] J. Wang, L. Yang, M. Sun, T. Liu, H. Li, Effect of energy input on the microstructure and properties of butt joints in DP1000 steel laser welding, Mater. Des. 90 (2016) 642–649. https://doi.org/10.1016/j.matdes.2015.11.006

[8] K. Bandyopandhyay, S. K. Panda, D. C. Saha, V. H. Baltazar-Hernandez, Y. N. Zhou, Microstructures and failure analyses of DP980 laser welded blanks in formability context, Mater. Sci. Eng. A 652 (2016) 250–263. https://doi.org/10.1016/j.msea.2015.11.091

[9] Q. L. Cui, D. Parkes, D. Westerbaan, S. S Nayak, Y. Zhou, D. Liu, F. Goodwin, S. Bhole, D. L. Chen, Effect of coating on fiber laser welded joints of DP980 steels, Mater. Des. 90 (2016) 516–523. https://doi.org/10.1016/j.matdes.2015.10.098

[10] A. K. Pramanick, H. Das, J. W. Lee, Y. Jung, H. H. Cho, S. T. Hong, M. Shome, A. K. Pramanick, Texture analysis and joint performance of laser-welded similar and dissimilar dual-phase and complex-phase ultra-high-strength steels, Mater. Charact. 174 (2021) 111035. https://doi.org/10.1016/j.matchar.2021.111035

[11] P. Švec, A. Schrek, M. Dománková, Microstructural characteristics of fibre laser welded joint of dual phase steel with complex phase steel, Kovove Mater. 56 (2018) 29–40. https://doi.org/10.4149/km_2018_1_29

[12] M. Morawiec, M. Rózański, A. Grajcar, S. Stano, Effect of dual beam laser welding on microstructure–property relationships of hot-rolled complex phase steels, Arch. Civ. Mech. Eng. 17 (2017) 145–153. https://doi.org/10.1016/j.acme.2016.09.007

[13] M. Rossini, P. Russo Spena, L. Cortese, P. Matteis, D. Firrao, Investigation on dissimilar laser welding of advanced high strength steel sheets for the automotive industry, Mater. Sci. Eng. A 628 (2015) 288–296. https://doi.org/10.1016/j.msea.2015.01.037

[14] E. A. Ariza, M. Masoumi, A. P. Tschiptschin, Improvement of tensile mechanical properties in a TRIP-assisted steel by controlling of crystallographic orientation via HSQ&P processes, Mater. Sci. Eng. A 713 (2018) 223–233. https://doi.org/10.1016/j.msea.2017.12.046

[15] J. J. Guzman-Aguilera, C. J. Martinez-Gonzalez, V. H. Baltazar-Hernandez, S. Basak, S. K. Panda, M. H. Razmpoosh, A. Gerlich, Y. Zhou, Influence of SC-HAZ microstructure on the mechanical behavior of Si-TRIP steel welds, Mater. Sci. Eng. A 718 (2018) 216–227. https://doi.org/10.1016/j.msea.2018.01.108

[16] E. Evin, M. Tomáš, The influence of laser welding on the mechanical properties of dual phase and trip steels, Metals 7 (2017) 239. https://doi.org/10.3390/met7070239

[17] Y. Wu, Y. Guo, W. Zhang, L. Li, Microstructure evolution and dynamic mechanical behavior of laser welded dissimilar joint between QP1180 and TRIP780, Journal of Materials Research and Technology, 16 (2022) 977–987. https://doi.org/10.1016/j.jmrt.2021.12.076

[18] Q. Lang, X. Zhang, G. Song, L. Liu, Effects of different laser power and welding speed on the microstructure and mechanical properties of TRIP joints laser-TIG arc hybrid lap filler wire welding, Mater. Today Commun. 29 (2021) 102925. https://doi.org/10.1016/j.mtcomm.2021.102925

[19] L. Mujica, S. Weber, H. Pinto, C. Thomy, F. Vollertsen, Microstructure and mechanical properties of laser-welded joints of TWIP and TRIP steels, Mater. Sci. Eng. A 527 (2010) 2071–2078. https://doi.org/10.1016/j.msea.2009.11.050

[20] Y. Najafi, F. Malek Ghaini, Y. Palizdar, S. Gholami Shiri, M. Pakniat, Microstructural characteristics of fusion zone in continuous wave fiber laser welded Nb-modified δ-TRIP steel, J. Mater. Res. Technol. 15 (2021) 3635–3646. https://doi.org/10.1016/j.jmrt.2021.09.116

[21] M. Merklein, M. Johannes, M. Lechner, A. Kuppert, A review on tailored blanks–Production, applications and evaluation, J. Mater. Process. Technol. 214 (2014) 151–164. https://doi.org/10.1016/j.jmatprotec.2013.08.015

[22] U. Reisgen, M. Schleser, O. Mokrov, E. Ahmed, Optimization of laser welding of DP/TRIP steel sheets using statistical approach, Opt. Laser Technol. 44 (2012) 255–262. https://doi.org/10.1016/j.optlastec.2011.06.028

[23] R. S. Sharma, P. Molian, Yb:YAG laser welding of TRIP780 steel with dual phase and mild steels for use in tailor welded blanks, Mater. Des. 30 (2009) 4146–4155. https://doi.org/10.1016/j.matdes.2009.04.033

[24] E. Zdravecká, J. Slota, Mechanical and microstructural investigations of the laser welding of different zinc-coated steels, Metals 9 (2019) 91. https://doi.org/10.3390/met9010091

[25] J. H. Lee, S. H. Park, H. S. Kwon, G. S. Kim, C. S. Lee, Laser, tungsten inert gas, and metal active gas welding of DP780 steel: Comparison of hardness, tensile properties and fatigue resistance, Mater. and Des. 64 (2014) 559–565. https://doi.org/10.1016/j.matdes.2014.07.065

[26] T. Wang, M. Zhang, R. Liu, L. Zhang, L. Lu, W. Wu, Effect of welding speed on microstructure and mechanical properties of laser-welded transformation induced plasticity (TRIP) steels, J. Iron Steel Res. Int. 27 (2020) 1087–1098. https://doi.org/10.1007/s42243-020-00397-x

[27] P. Švec, A. Schrek, M. Dománková, Microstructure evolution of fibre laser welded TRIP and HSLA steel sheets with different thicknesses, Kovove Mater. 57 (2019) 219–227. https://doi.org/10.4149/km_2019_4_219